Oxidation of Ni-Cr alloy at intermediate oxygen pressures. I. Diffusion mechanisms through the oxide layer

Eric Schmucker, Carine Petitjean, Laure Martinelli, Pierre-Jean Panteix, Sabah Ben Lagha, Michel Vilasi

Oxidation of Ni-Cr alloy at intermediate oxygen pressures. I. Diffusion mechanisms through the oxide layer

Eric Schmucker[a,c*], Carine Petitjean[a], Laure Martinelli[b], Pierre-Jean Panteix[a], Sabah Ben Lagha[c], Michel Vilasi[a]

[a] *IJL-UMR 7198, Département CP2S, Equipe 206 (Surface et Interface: Réactivité Chimique des Matériaux), B.P. 70239 – F-54506 Vandœuvre les Nancy Cedex, FRANCE.*

[b] *CEA, Université Paris-Saclay, Den-Service de la Corrosion et du Comportement des Matériaux dans leur Environnement (SCCME), F-91191, Gif-sur-Yvette, FRANCE.*

[c] *AREVA NC, Tour Areva, 1 Place Jean Millier, F-92084, Paris-La-Défense Cedex, FRANCE*

*corresponding author
e-mail: eric.schmucker@univ-lorraine.fr; phone: + 33 (0) 3 83 68 46 69; fax: + 33 (0) 3 83 68 46 11

Abstract

The oxidation of Ni-30Cr alloy has been studied at 1150 °C up to 289 h at oxygen pressures comprised between 10^{-13} and 10^{-3} atm in Rhines pack. This method allows the determination of the sole Cr_2O_3 growth kinetics at reduced oxygen pressure without the use of reactive gas mixture. Oxide morphology, growth mechanisms and kinetics are discussed in terms of nature, concentration and diffusion of point defects. Diffusion coefficients are calculated from the oxidation kinetics data. Moreover, the transition from interstitials to vacancies diffusion mechanism for the oxide growth is discussed.

Keywords: A. alloy; B. SEM; C. high temperature corrosion; C. oxidation; C. kinetic parameters.

Introduction

In many high temperature applications, e.g. nuclear wastes vitrification [1], heat exchangers or gas burners [2], metallic components are submitted to high thermal and mechanical loads. Ni-based superalloys with high Cr content, generally comprised between 15 and 30 wt.%, are candidate materials for such applications. When oxidised, these kinds of alloys are able to

develop a protective, slow-growing chromium oxide (Cr_2O_3) scale that can withstand different types of corrosion, e.g. by hot gases, molten glass or salts. Moreover, mechanical strengthening can be obtained by the addition of carbides in the alloy matrix [3].

Oxidation of binary Ni-Cr alloys with more than 25 wt.% Cr usually leads to the formation of exclusive Cr_2O_3 with small amount of NiO generated during transient oxidation [4-6]. The growth kinetics of this oxide, at steady-state conditions, generally obeys a parabolic law in agreement with Wagner's theory of oxidation [7] or paralinear law if oxidation of Cr_2O_3 into volatile $CrO_{3(g)}$ occurs [8]. Indeed, oxidation of Cr_2O_3 into $CrO_{3(g)}$ can be encountered at temperatures above 1000 °C and is enhanced in high-$P(O_2)$ environment and by high gas velocity [9,10]. The growth of Cr_2O_3 in O_2 atmospheres generally occurs at the scale/gas interface by outward diffusion of cations [11-15], along short-circuit paths like grain boundaries [4,16]. However a change in the nature of the environment [15,17] (e.g. addition of water vapor) or the addition of reactive elements [13] (e.g. rare earth elements) can induce a change in growth mechanism and lead to consequent or even main inward diffusion. Many authors have investigated the diffusion of chromium and oxygen in Cr_2O_3 and most of them have found that chromium diffusion was faster than oxygen diffusion [11,12,18,19], even though Sabioni *et al.* have found a greater diffusion coefficient for oxygen in Cr_2O_3 [20]. Thus, outward growth of the scale can be attributed to faster diffusion of chromium in the oxide. The presence of water can affect the defects structure of the oxide by injection of protons [21]. Henry *et al.* have attributed the increase of scale growth rates to the smaller ionic radius of OH^- species (95 pm) compared to O^{2-} ions (140 pm) [17]. The effect of reactive element like yttrium or cerium is often seen as segregation at grain boundaries, thus blocking fast diffusion and reducing the scale growth rate [22]. Another consequence of the doping by reactive elements is a donor effect which leads to an increase of oxygen defects concentration or to a decrease in chromium defects concentration [22] leading to faster diffusion of oxygen [16]. Since the oxygen activity has a great impact on the defects structure of chromium oxide and their diffusivities [11] and that various oxygen pressures can be encountered in the different corrosive environments, it is of interest to focus on the effect of the oxygen pressure on the high temperature oxidation of chromia-forming alloys. As a consequence of the wide oxygen activity difference throughout Cr_2O_3 scales, both chromium vacancies and interstitials can exist. Hindam and Whittle [23], in atmospheres between 10^{-14} and 10^{-8} atm O_2 imposed by CO_2/CO mixtures at 1000 °C, as well as Kofstad and Lillerud [18], in different $P(O_2)$ from 7 x 10^{-7} up to 1 atm at 1000-1100 °C, have shown that chromium

interstitials were responsible for the transport of matter in the oxide, controlling the oxidation kinetics of pure chromium. Ramanarayanan *et al.* [24] have also considered chromium interstitials defects in oxide grown on Ni-30Cr alloy at 900-1125 °C in CO_2/CO mixtures. On the contrary, some authors have also considered vacancies as the main or possible defects in Cr_2O_3 in very different atmospheres like oxygen (> 0.1 atm) [16] or low-$P(O_2)$, H_2-H_2O mixture at 800-900 °C [25].

In this paper, the oxidation kinetics and mechanism of a model Ni-30Cr alloy at 1150 °C in several intermediate oxygen partial pressures $P(O_2)$, from 10^{-13} atm up to 10^{-3} atm, are described. A specific feature of this work is to achieve a method for the determination of the sole growth kinetics of an oxide layer. Indeed such information can be useful for the study of corrosion kinetics of alloys by molten phases (e.g. molten glass or molten salts), in order to decorrelate the oxide growth from its destruction by corrosive media [26]. Therefore, oxidation tests have been carried out with the Rhines pack method. This method was introduced by Rhines in 1940 [27]. It allows the control of the oxygen pressure in a sealed reactor at elevated temperature, thanks to the equilibrium established between powders of a metal/oxide redox couple. It has been generally used for the study of internal oxidation and oxygen transport in alloys [28-30]. Surprisingly, it has not been used for the study of external oxidation kinetics up to now. Yet, the advantages of this method are crucial: (i) to get rid of the effect of hydrogen or carbon doping when using H_2O/H_2 or CO_2/CO mixtures to impose low oxygen partial pressures; (ii) to avoid the oxidation of Cr_2O_3 into volatile CrO_3 (see details in the next section). Thus, oxidation kinetics obtained in this work are the sole growth kinetics in O_2 atmospheres. Furthermore, an original method for the determination of the diffusion coefficients of chromium and chromium permeability in Cr_2O_3 layer is detailed. This method is based on the exploitation of the oxidation kinetics data. Reviews of the available data in the literature concerning parabolic rate constants for the oxidation of Ni-based chromia-formers and diffusion coefficients in Cr_2O_3 are made. The attention is primarily focused on the effect of the oxygen pressure. A diffusion mechanism, based on experimental results and literature, is established and may account for the oxidation of model chromia-forming alloys in reduced oxygen pressure.

Materials and methods

The Ni-30Cr (wt.%) alloy was synthesised by high frequency induction under argon atmosphere (< 2 ppm O_2). Pure chromium (99.99% purity) and nickel (99.95% purity) from Alfa Aesar were used as base components. The composition of the alloy was verified by EDX analyses and the chromium content was found to be equal to 30.5 ± 1.2 wt.%. For this composition and at temperatures higher than 800 K, this alloy is a single phased, austenitic (f.c.c.), solid solution of chromium in nickel [31]. The microstructure of the alloy is coarse with a grain size of several hundreds of micrometres (as shown in part II of this work [32]).

For the oxidation tests, samples were cut from the ingot with dimensions around 8 x 8 x 1.5 mm and ground with P1200 SiC paper. Oxidation experiments have been performed with controlled oxygen partial pressures in Rhines packs (Fig. 1). Ni-30Cr samples and metal/oxide powders mixtures were placed in separated alumina crucibles and then encapsulated in a ~10 cm^3 silica tube sealed in secondary vacuum. Metal/oxide and oxide/oxide buffers impose a specific oxygen partial pressure at a given temperature thanks to the thermodynamic equilibrium between two MO_ν species with $\nu \geq 0$ (Eq. 1).

$$MO_a + \frac{b-a}{2} O_2 = MO_b \qquad \text{Equation 1}$$

Metal/oxide and oxide/oxide buffers used for the oxidation tests are listed in Table 1 with the corresponding imposed equilibrium pressure of oxygen at the test temperature of 1150 °C. After oxidation experiments, the presence of both phases in the buffers was checked by XRD measurements in order to confirm that the desired $P(O_2)$ have been thermodynamically imposed all along the experiment. The oxygen consumption rate to form the oxide layer on Ni-30Cr sample is very low (because it is limited by solid state diffusion in the oxide) compared to the reaction rate between MO_ν species or compared to the diffusion rate through the gas phase. Therefore the presence of both phases in the buffers after experiment is a reliable indicator that the oxygen pressure did not change in the reactor during the experiment. Moreover, an estimation of the quantity of Cr_2O_3 oxidised into $CrO_{3(g)}$ according to Eq. 2 is made for the different oxygen partial pressures.

$$Cr_2O_{3(s)} + \frac{3}{2} O_{2(g)} = 2CrO_{3(g)} \qquad \text{Equation 2}$$

The saturation pressures of CrO_3 have been calculated from the Gibbs energy of Eq. 2 and are listed in Table 1. With the application of the ideal gas law, by considering a reactor volume of about 10 cm^3, the amount of chromium that transformed from Cr_2O_3 into $CrO_{3(g)}$ can be

estimated and is found to be negligible compared to the mass gain after oxidation (less than 10^{-6} mg for the highest $P(O_2)$ compared to a few milligrams uptake). Thermodynamic calculations have been made with HSC software [33] using databases from [34-38]. Thus, the use of such a device drastically decreases the importance of Cr_2O_3 oxidation due to the limited volume of the reactor, low oxygen pressure and static gas conditions.

Several oxidation tests have been performed in a muffle furnace from 1 h to 289 h at 1150 °C. Samples were placed in the furnace directly at test temperature and directly quenched in air after oxidation. Surface characterisations (Scanning Electron Microscopy (SEM) and X-Ray Diffraction (XRD)) have been performed before embedding in epoxy resin and grinding up to mirror polishing for cross-section observations. Some samples were polished with an ionic polisher (JEOL IB-09010CP) rather than mechanically in order to obtain a neater surface preparation for observation. For inert markers experiments, a 15 nm thin gold layer was deposited at the surface of the samples by pulverization. In order to avoid the gold diffusion in the alloy during the high temperature oxidation, a short oxidation of the Ni-30Cr samples at 700 °C during 3 h was performed prior to the gold deposition. This oxidation led to the formation of a very thin (~100 nm) oxide layer.

XRD characterisations of buffers and oxidised samples have been performed with an X'pert Pro MRD diffractometer with a copper anticathode (λ $CuK\alpha_1$ = 1.5406 Å). *In-situ* high temperature XRD measurements have been performed at 1100 °C in air with a D8 Discover diffractometer with a cobalt anticathode (λ $CoK\alpha_1$ = 1.7900 Å). SEM observations have been performed with a tungsten filament JEOL 6010LA and a field-effect, Schottky emission JEOL J7600F microscopes. Oxidation kinetics were assessed in terms of oxide thickness variation and values were obtained from an average of 15 measurements on each face of a sample.

Results

1. Morphology of oxide scale

The morphology of the oxide formed on Ni-30Cr alloy after oxidation at 1150 °C is shown in Fig. 2a to d and Fig. 3 for different oxygen partial pressures and times. EDX analyses indicate that the scale is constituted of chromium oxide Cr_2O_3 with small amount of doping nickel,

especially for short oxidation duration. The presence of nickel in the scale, while only chromium oxide should be formed for such Cr content in the alloy [4,6,39], comes from the transient oxidation step. The concentration of nickel in Cr_2O_3 was always found to be less than 1 wt.%, an extent of solubility previously reported by Davies and Smeltzer in Ni-$NiCr_2O_4$-Cr_2O_3 phases equilibrium at 1000-1100 °C [5]. In Fig. 2b and d, swelling lines are visible and are coherent with the shape and size of the alloy grain boundaries underneath. Except for the presence of few pores within the oxide, the scale is dense, compact and adherent to the metal (Fig. 3). In addition, the oxide microstructure can also be distinguished and consists of small micrometric grains. The clear spots in the oxide near the alloy/oxide interface are enriched in nickel and are therefore most probably vestiges of a former location of the alloy (Fig 3). Alloy recession can be explained either by an inward growth contribution or by vacancies annihilation at the alloy/oxide interface [32]. Important desquamation of the oxide occurred only on samples oxidised in the highest $P(O_2)$ (Fig. 2a and b) and the number of spalling sites increased with increasing oxidation duration. Spallation occurred during the quenching of the samples and was always located along the alloy grain boundaries (Fig. 2b) leaving bare alloy at the surface (Fig. 2a).

XRD measurements have been performed on the surface of the oxidised samples and have confirmed that the oxide is made of a single hexagonal phase of Cr_2O_3 (Fig. 4). The oxide spallation for the highest $P(O_2)$ is also evidenced here with the apparition of diffraction peaks of the alloy. Peaks indexation has indicated that the chromium oxide lattice is distorted with an increase of 0.8% of the a and b parameters, and an increase of 0.3% of the c parameter compared to data of reference [40]. This distortion can be consequence of thermal expansion and growth strains created during high temperature oxidation that are kept at room temperature due to the quenching of the samples. Cr_2O_3 (hk0) textured growth is observed (Fig. 4) and Fig. 5 evidences the decrease of the (104) peak and the increase of the (110) peak after a few hours of oxidation in air at 1100 °C. This result is in contrast with those of Henry *et al.* who have stated a (001) orientation on pure chromium oxidised in O_2 at 900 °C [17].

2. Inert markers experiments

Results from inert markers experiments are shown in Fig. 6a and b for the two extreme oxygen partial pressures respectively equal to 5.9×10^{-3} and 2.8×10^{-13} atm. Markers

experiments have also been performed for the other $P(O_2)$ and whatever the oxygen partial pressure was, gold markers have always been found close to the alloy/oxide interface after 9 h of oxidation. This location indicates that the oxide scale grew mainly by outward diffusion of chromium species. External growth of chromium oxide has already been reported by several authors on high-chromium alloys by platinum markers [14] or on binary alloy like Ni-25Cr by O^{18} isotopic tracers [13,15]. Nonetheless, Zurek *et al.* [15] have found exclusive outward growth on Ni-25Cr in air at 1050 °C while Beske *et al.* [13] have also found additional inward growth contribution for the same alloy composition in air at 1000 °C. Yet, at 1000 °C, the formation of nickel chromium spinel has been observed at the oxide/atmosphere interface.

3. Oxidation kinetics

The oxide thickness variations *vs* time on Ni-30Cr alloys oxidised at 1150°C for all tested oxygen partial pressures are shown in Fig. 7. The evolution of the oxide thickness is very similar whatever the oxygen partial pressure is, ranging from ~5 µm after 1 h of oxidation up to 35-40 µm after 289 h of oxidation. The oxide thickness variation curves can be fitted with the complete law for parabolic oxidation [41]:

$$t = t_i - \frac{x_i^2}{2k_{pe}} + \frac{1}{2k_{pe}}x^2 \qquad \text{Equation 3}$$

where t is the oxidation duration in s, t_i and x_i are respectively the time in s and the oxide thickness in cm from which the parabolic oxidation starts. x is the oxide thickness in cm at time t and k_{pe} represents the parabolic rate constant for the oxidation in $cm^2\ s^{-1}$. Parabolic rate constants k_{pe} were obtained with the help of Eq. 3 by plotting the time t versus the oxide thickness x and are listed in Table 2. Fig. 7a shows good agreement between the experimental results and the parabolic curve fitted with an average k_{pe} value equal to 5.0×10^{-12} $cm^2\ s^{-1}$. The parabolic behaviour is confirmed by the linear plot of x versus the square root of time on Fig. 7b. Parabolic behaviour is consistent with a diffusion controlled process in near-stoichiometric Cr_2O_3 according to Wagner's theory. The average k_{pe} value is listed in Table 3 with other key parameters for the oxidation kinetics determined afterwards.

Discussion

1. Oxide scale characteristics

The knowledge of chromium oxide point defects structure is convenient for the comprehension of the morphological and kinetic phenomena occurring during the oxidation of Ni-Cr alloys. At temperatures above 1000-1200 °C, Cr_2O_3 is known to be an intrinsic electronic semi-conductor [42] but ionic defects responsible for oxide growth (chromium/oxygen vacancies/interstitials) can coexist and their concentrations are dependent of the oxygen pressure through the oxide scale [11]. Fig. 8 represents the Brouwer diagram of Cr_2O_3 at 1100 °C according to Su and Simkovich [43]. It can be seen that when the external oxygen pressure is inferior to about 10^{-10} atm, the main cationic defects throughout the whole scale thickness are chromium interstitials. This situation corresponds to the oxidation tests with the three lowest $P(O_2)$ in this work. Oxygen pressure imposed by Fe_2O_3/Fe_3O_4 buffer induces a much wider oxygen pressure difference throughout the scale. Therefore, for tests in high $P(O_2)$, both cationic defects *i.e.* vacancies and interstitials, can exist throughout the scale, with vacancies preponderance near the oxide/atmosphere interface and interstitials dominating near the alloy/oxide interface.

An obvious difference in the scale morphology when the alloy is oxidised either in low or in high oxygen partial pressure is the strong extent of spallation occurrence during cooling on samples oxidised in high $P(O_2)$, while in the low $P(O_2)$ scales remained almost intact (Fig. 2a to d). Moreover spallation sites are located above grain boundaries of the alloy. First of all, it is well known that oxide scales are submitted to compressive growth stresses during oxidation and thermal stresses upon cooling [44,45]. In this way, compressive stresses are increasing with higher oxide thickness. Thermal stresses are due to the mismatch between the coefficients of thermal expansion of the oxide and the alloy. Thus, thermal stresses increase with higher temperature difference during cooling [44]. Indeed, Berthod *et al.* have observed extended oxide spallation during oxidation of Ni-25Cr alloy when increasing test temperature or oxide thickness [46]. Since the test temperature is unique in the present study, thermal stresses should be the same in all tested atmospheres and cannot account for the difference in spallation occurrence depending on the oxygen pressure. Therefore a change in growth mechanism of the oxide should explain this difference. As seen in Fig. 8, the defect structure of Cr_2O_3 is very similar for the three low $P(O_2)$ while it differs for the high $P(O_2)$ used in this

study. At high oxygen activities, diffusion of oxygen interstitials species (in addition to chromium vacancies) can become significant in the outer part of the oxide layer, thus leading to a counter-current mechanism for the oxide growth. In that case, the formation of the oxide would take place within the scale, thus generating more stresses [11]. Failure of the scale can happen on interfacial flaws when the oxide is under compression [44,47]. This explains why spallation occurs above the alloy grain boundaries where chromium is more rapidly brought from the alloy and injected in the oxide scale. Indeed, this can induce slightly higher growth rate and stresses on these specific sites.

Another morphological difference is the presence of more porosities in the oxide scale after oxidation in the high $P(O_2)$ (Fig. 6a and b). Pores are generally supposed to arise from the accumulation of vacancies [48,49]. Therefore it is not surprising to obtain more porosities in the high $P(O_2)$ atmosphere since the presence of chromium vacancies is more significant in this case. At low $P(O_2)$, chromium vacancies can still exist, even if it has very low concentration, therefore the formation of few porosities is still possible, but with a limited extent (Fig. 8).

In conclusion, it appears that the mechanical characteristics of the oxide layer are dependent on the oxygen pressure. At high $P(O_2)$, important desquamation of the oxide scale can occur during cooling due to higher growth stresses. These stresses may be induced by the increased contribution of inward oxygen diffusion.

2. Oxidation kinetics

As seen in Table 2, values of k_{pe} are all very close in the same order of magnitude and consistent with those of chromia-forming materials. A data review in Fig. 9 compares the values obtained in this work with parabolic rate constants of chromia-forming Ni-based alloys from other authors. Data are gathered from works on oxidation of commercial alloys [50-52] and binary Ni-Cr alloys (> 20 wt.%Cr) in different atmospheres: oxygen [16,53], air [8,39,45,46,50,54], argon-oxygen mixture [6] or CO_2/CO mixture [24]. Results from Calvarin *et al.* have been obtained with 100 or 200 µm thin Ni-20Cr foils [54]. Li *et al.* have studied the oxidation kinetics in air of Ni-27.8Cr alloyed or not with additional elements [50]. Ecer *et al.* [14], Moulin *et al.* [53] and Hodgkiess *et al.* [55] have studied the oxidation kinetics of

high-chromium alloys, and pure chromium for Wood *et al.* [56]. They have found higher oxidation rates than those for "optimal" compositions of about 25-30%. Essuman *et al.* [6], Berthod *et al.* [46] and Hänsel *et al.* [57] have compared the oxidation kinetics of binary Ni-25Cr alloy in dry and wet atmospheres. Finally, the addition of rare-earth reactive elements like yttrium or cerium has proved to induce a decrease of the oxidation rate of alloys [16,24,58].

Conclusions about the effect of the chromium content in the alloy on the oxidation rate can be quite easily drawn from Fig. 9 (oxidation rate of alloy, from lowest to highest: Ni-25Cr ≤ Ni-30Cr < Ni-20Cr < high-chromium alloys). Unfortunately, the effect of oxygen pressure is more sensitive given that parameters and experimental methods are few comparable between different studies. Nevertheless, for alloy composition Ni-30Cr, it seems that oxidation rates in high $P(O_2)$ (≥ 0.1 atm) [8,16] and especially [53] are greater than those found in the present work with intermediate oxygen partial pressures. In low $P(O_2)$ CO_2/CO mixture (10^{-18}-10^{-15} atm O_2 at 900-1050°C), Ramanarayanan *et al.* [24] have also obtained higher growth rates but the nature of the atmosphere is different. Finally, our results are consistent with the data of the literature, as k_p values are similar to those of Ni-25Cr or Ni-30Cr alloys. Yet, lower oxidation rates might be reached in intermediate oxygen pressures.

Fig. 10a and b show the evolution of the parabolic rate constant k_{pe} versus time during the oxidation. In this case, the k_{pe} values (calculated from the slope between a time t_n and t_{n+1}) have been obtained by using the classic linear equation for parabolic oxidation:

$$k_{pe} = \frac{1}{2}\left(\frac{x_{n+1} - x_n}{\sqrt{t_{n+1}} - \sqrt{t_n}}\right)^2 \qquad \text{Equation 4}$$

The oxidation rate quickly decreased during the first hours of oxidation and it appears that a steady-state regime is achieved after more than 25-49 hours of oxidation. Moreover, whatever the oxygen partial pressure is, the parabolic rate constants at steady-state are similar to those determined with Eq. 3, *i.e.* 5.0 x 10^{-12} cm^2 s^{-1}.

3. Diffusion through the oxide layer

3.1. Oxidation mechanism

The k_{pe} values obtained from Eq. 3 are plotted versus the logarithm of oxygen pressure in Fig. 11. According to Wagner's theory of oxidation, the parabolic rate constant can vary with the oxygen pressure depending on the nature of the diffusing defect. From inert markers experiments, cationic growth is evidenced (Fig. 6a and b). Therefore, by considering triply charged chromium cations, k_{pe} constants can be expressed by Eq. 5 and 6 depending on the defect nature (in the case of an intrinsic electronic semi-conductor) [11].

Chromium vacancies V_{Cr}''' $$k_{pe} = const.\left[\left(P_{O_2}^{ext}\right)^{\frac{3}{4}} - \left(P_{O_2}^{int}\right)^{\frac{3}{4}}\right]$$ Equation 5

Chromium interstitials $Cr_i^{\bullet\bullet\bullet}$ $$k_{pe} = const.\left[\left(\frac{1}{P_{O_2}^{int}}\right)^{\frac{3}{4}} - \left(\frac{1}{P_{O_2}^{ext}}\right)^{\frac{3}{4}}\right]$$ Equation 6

At 1150 °C, the oxygen pressure, calculated with HSC software [29,31,33], for Cr_2O_3/Ni-Cr equilibrium at the alloy/oxide interface is about 9.6 x 10^{-19} atm (the interfacial chromium content at steady state being equal to 23 wt.% [32], the corresponding chromium activity, computed with Thermo-Calc/SSOL4 database [59], is equal to 0.29). This is several orders of magnitude below external oxygen pressures used for oxidation experiments. Thus, Eq. 6 indicates that k_{pe} is independent of the external oxygen pressure if chromium interstitials are responsible for scaling kinetics. However, an increase of k_{pe} with the oxygen pressure is expected if chromium vacancies are diffusing (Eq. 5). The dashed lines in Fig. 11 represent theoretical evolutions for each type of defect. It clearly appears that the parabolic rate constant for oxidation of Ni-30Cr alloy at 1150 °C is independent of the $P(O_2)$ in the range of oxygen partial pressure from 10^{-13} up to 10^{-3} atm O_2.

As a consequence, it is concluded that diffusion of chromium interstitials species is controlling the oxidation kinetics of Ni-30Cr alloy in oxygen atmospheres comprised between 10^{-13} and 10^{-3} atm O_2 at 1150 °C.

This conclusion is in accordance with other authors who have suggested chromium interstitials diffusion as the rate-controlling process in oxidation of chromia-formers in intermediate or low oxygen pressures [18,23,24]. However, from oxidation tests in high $P(O_2)$ pure oxygen (≥ 0.1 atm), Tsaï *et al.* have deduced that diffusion of chromium vacancies is the rate-controlling process [16]. Moreover, a study on the oxidation mechanism of alloy Inco 690 in 10^{-6} and 0.2 atm O_2 at 700 °C has revealed that the oxide growth was controlled by

chromium vacancies diffusion in the high $P(O_2)$ atmosphere and by chromium interstitials in the lower $P(O_2)$ atmosphere [60]. Some authors have found anionic diffusion in Cr_2O_3 formed on chromia-forming alloys [13,51], but they observed the presence of a $MnCr_2O_4$ or $NiCr_2O_4$ spinel in the outer part of the oxide scale. On the contrary, Zurek *et al.* [15] have not observed any change in the cationic growth mechanism between Ni-25Cr and Ni-25Cr-Mn alloys oxidised in Ar-20%O_2 atmosphere, although the spinel phase was present after oxidation of the Mn-containing alloy. The equilibrium between the spinel phase and Cr_2O_3 is likely to impose an intermediate oxygen partial pressure at their junction [61], but the reason for a change from cationic to anionic mechanism remains unclear.

The establishment of a criterion for the transition from chromium interstitial to chromium vacancy diffusional mechanism is now discussed. The criterion for this transition can be seen as a competition between the relative extent of chromium interstitials and vacancies concentration gradients through the oxide layer. These gradients are mainly impacted by the defect concentration at the alloy/oxide interface and at the oxide/atmosphere interface respectively. According to the Cr_2O_3 Brouwer diagrams [43], the following features can be expected: (i) for a fixed external oxygen pressure, the vacancies concentration at the oxide/atmosphere interface gradually exceeds the interstitials concentration at the alloy/oxide interface with increasing temperature; (ii) an increase of the external oxygen pressure results in an increase of the vacancies concentration; (iii) a decrease of the chromium activity results in a higher oxygen pressure at the alloy/oxide interface (Eq. 1) and therefore results in a lower interstitials concentration. Fig. 12 shows the different cationic mechanisms determined in this work and given by other authors [16,18,23,24,60] in a temperature *vs.* external oxygen pressure graph. A boundary (grey dashed line) between the interstitial type and the vacancy type domains can be drawn. This boundary is consistent with the above consideration on the chromium vacancies/interstitials predominance.

In conclusion, it appears that the transition between the chromium interstitial mechanism and the chromium vacancy mechanism for oxidation can be drawn depending on temperature and external oxygen pressure (Fig. 12). A vacancy type mechanism is favoured, (i) at higher oxygen pressure, (ii) at lower temperature and (iii) for lower chromium activity in the alloy.

3.2. Determination of diffusion coefficients

The growth of an oxide layer generally involves many parameters like the nature of the defects, their concentrations and the oxide microstructure. In order to interpret the oxide growth kinetics in terms of diffusion, it is convenient to get an insight on the concentration and the diffusion coefficient of the main defect. In the present case, it is shown that the oxide grew by diffusion of chromium interstitials species. Moreover, the oxide has a fine microstructure with a micrometric grain size (Fig. 3), making predominant rapid diffusion along grain boundaries possible.

Fig. 13 summarizes data from literature of chromium diffusion coefficient D_{Cr} in Cr_2O_3 [16,19,62-69] and a great disparity of values is clearly visible. Nevertheless, two domains can be distinguished: a first one, with the lowest values, corresponds to diffusion coefficients in bulk oxide (square symbols). The second one corresponds to short-circuit or mixed diffusion coefficients (triangles or diamond-shaped symbols respectively).

Most of the diffusion coefficients in literature have been obtained by isotopic tracer experiments in Cr_2O_3 single crystals or polycrystals [19,58-60,63,65]. Therefore these coefficients represent tracer diffusion coefficients D^*_{Cr} [70]. Measurements from Atkinson and Taylor [63] at 1100 °C in a wide range of oxygen activities (5×10^{-20} up to 0.2) have revealed that diffusion of chromium in Cr_2O_3 single crystal is made by interstitials diffusion in low oxygen activities and by vacancies diffusion in high oxygen activities. At higher temperature (1570 °C), Hoshino and Peterson [64] have found a vacancy mechanism for chromium diffusion in oxygen activities between 8×10^{-10} and 1×10^{-5}. Tsai *et al.* [16,19] have determined diffusion coefficients in a Cr_2O_3 polycrystal and in a Cr_2O_3 scale grown on Ni-30Cr in 0.1 atm O_2 by isotopic tracer experiments. At 900 °C, the value obtained for diffusion in grain boundaries is higher in scale than those in polycrystal. This difference may be explained by the fact that in the oxide scale, besides the stochastic diffusion of the tracer, there is an additional driving force for the diffusion which is the chemical potential gradient of chromium. For that reason, their diffusion coefficients in Cr_2O_3 scales might not be tracer diffusion coefficient but intrinsic diffusion coefficient $\tilde{D}_{Cr}$ [70]. Moreover, based on the evolution of the parabolic rate constant with the oxygen pressure, the authors have concluded

that the diffusion of chromium occurs by a vacancy mechanism. In addition, they have also estimated apparent diffusion coefficients D_{app}, taking into account the microstructure of the oxide, by mixing grain boundaries diffusion coefficient D_{gb} and bulk diffusion coefficient D_B with Eq. 7, where f is the fraction of surface sites associated with grain boundaries and depends on the grain size and grain boundary width (the grain boundary width is generally assumed to be about 1 nm) [16,19].

$$D_{app} = (1 - f)D_B + fD_{gb} \qquad \text{Equation 7}$$

Hagel and Seybolt [69] have determined the diffusion coefficient of chromium in hot-pressed and sintered Cr_2O_3 polycrystals from 1045 up to 1550 °C. Their tracer diffusion experiments were carried out in nitrogen (about 10^{-6} atm O_2). Owing to the strongly reducing conditions used during the hot-pressing elaboration of Cr_2O_3 in graphite dies, their hot-pressed samples contained small amount of metallic chromium. Thus, for hot-pressed Cr_2O_3, their results reflect diffusion near Cr-Cr_2O_3 phase boundary *i.e.* by an interstitial mechanism at low oxygen activity [11]. However, since the synthesis of hot-pressed samples and the diffusion annealing have been carried out in different oxygen activities, a chemical potential gradient of oxygen could have been created between the core and the surface of the sample and therefore, due to this additional driving force, their diffusion coefficient in hot-pressed Cr_2O_3 might be intrinsic diffusion coefficients. Lebreau *et al.* have performed DFT calculations in order to evaluate self-diffusion coefficients D_{Cr} of chromium vacancies or interstitials in different directions in Cr_2O_3 lattice [65]. Kofstad and Lillerud [68] have annealed preoxidised Cr specimen in high vacuum, in a temperature range from 1100 up to 1300 °C, in order to follow the weight loss due to chromium transport through the scale. Assuming electronic or ionic defects predominance, they have obtained chromium self-diffusion coefficients D_{Cr} which are representative of diffusion by an interstitial type mechanism. It should be noted that self-diffusion coefficient and tracer diffusion coefficient are related by a correlation factor which is dependent on the presence of available neighbouring sites around the diffusing species. In the case of interstitial mechanism this correlation factor is close to unity and thus tracer diffusion coefficient $D^*_{Cr}$and self-diffusion coefficient D_{Cr} values are similar [70].

In order to discriminate which diffusion coefficient value amongst those in Fig. 13, is best corresponding with the oxidation kinetics obtained in this work, it is possible to calculate the permeability of chromium $N_{Cr_i}.\bar{D}_{Cr}$ through the scale, assuming that diffusion is carried out only by chromium interstitials. N_{Cr_i} is the concentration of chromium interstitials in Cr_2O_3 at

the alloy/oxide interface and $\bar{D}_{Cr}$ is the intrinsic diffusion coefficient of chromium in the oxide layer. This permeability can be calculated by two different ways:

(i) The first one is related to the parabolic rate constant for oxidation, according to Eq. 8 [61].

$$k_{pe} = \Omega \bar{D}_{Cr} \Delta N_{Cr_i} \qquad \text{Equation 8}$$

where Ω, the oxide volume created by one Cr atom is equal to 2.4 x 10^{-23} cm^3 at^{-1}. ΔN_{Cr_i} is the chromium interstitials concentration difference between internal and external interface in at cm^{-3}.

Since chromium interstitials are considered as the diffusing species and their concentration at the external interface is very small, the term ΔN_{Cr_i} in oxide can be simplified to N_{Cr_i}. Calculation with Eq. 8 made with k_{pe} = 5.0 x 10^{-12} cm^2 s^{-1}, results in a permeability $N_{Cr_i}.\bar{D}_{Cr}$ equal to 2.1 x 10^{11} at cm^{-1} s^{-1}.

(ii) The second one is obtained by assuming that in steady-state conditions, the chromium flux arriving from the alloy to the oxide layer is in first approximation equal to the chromium flux through the oxide layer. This is expressed by Fick's first law (the concentration gradient of total chromium in the oxide being equivalent to concentration gradient of chromium interstitials):

$$J_{Cr}^{alloy}\Big|_{x=0} = -\tilde{D}_{Ni-30Cr} \frac{\partial N_{Cr}^{alloy}}{\partial x_{alloy}}\Big|_{x=0} = J_{Cr}^{oxide} = -\bar{D}_{Cr} \frac{\partial N_{Cr_i}}{\partial x_{oxide}} \qquad \text{Equation 9}$$

where chromium fluxes J_{Cr} are expressed in at cm^{-2} s^{-1} and chromium concentration N_{Cr} in at cm^{-3}. $\tilde{D}_{Ni\text{-}30Cr}$ is the interdiffusion coefficient of chromium in the alloy, taken from [32], and is equal to 1.2 x 10^{-10} cm^2 s^{-1}. x_{oxide} is the oxide thickness in cm.

For calculation with Eq. 9, the oxide thickness, and the chromium concentration gradient in the alloy are required. These data are taken from part II of this work [32]: for instance, for a sample oxidised in 5.9 x 10^{-3} atm O_2 during 49 h, *i.e.* long enough to reach steady-state regime, the oxide thickness is equal to 18 x 10^{-4} cm. The chromium gradient obtained from the depletion profile is taken equal to -7.9 x 10^{23} at cm^{-4} (calculated from a difference of 2 wt.% of chromium over 20 µm next to the alloy/scale interface).

In this case, with the use of Eq. 9, the permeability $N_{Cr_i}.\bar{D}_{Cr}$ in Cr_2O_3 is equal to 1.7 x 10^{11} at cm^{-1} s^{-1}. Thus both methods are consistent and give comparable results roughly equal to 2 x 10^{11} at cm^{-1} s^{-1}.

Now, for the sake of comparison with data in Fig. 13, the intrinsic diffusion coefficient of chromium $\bar{D}_{Cr}$ must be expressed in function of tracer diffusion coefficient D^*_{Cr}. The flux of chromium in the oxide layer is expressed by the Fick's first law in Eq. 9. However, in the oxide layer, the chemical potential of chromium gradient is the real driving force for diffusion of chromium. The flux of chromium in the oxide (in at cm^{-2} s^{-1}) can then be expressed as [71]:

$$J_{Cr}^{oxide} = -B_{Cr}N_{Cr}\frac{\partial \mu_{Cr}}{\partial x} \qquad \text{Equation 10}$$

where N_{Cr} is the concentration of total chromium species in the oxide, equal to 4 x 10^{22} at cm^{-3}. B_{Cr} denotes the mobility of chromium which is connected to the tracer diffusion coefficient of chromium via the Nernst-Einstein relation:

$$D_{Cr}^{\bullet} = B_{Cr}RT \qquad \text{Equation 11}$$

where R is the ideal gas constant (in J mol^{-1} K^{-1}) and T the temperature in K.

By identification in Eq. 9, 10 and 11, the relation between the intrinsic and the tracer diffusion coefficient is:

$$\bar{D}_{Cr} = D_{Cr}^{\bullet}\frac{N_{Cr}}{RT}\frac{\partial \mu_{Cr}}{\partial N_{Cr_i}} \qquad \text{Equation 12}$$

The chemical potential of chromium μ_{Cr} in Cr_2O_3 is related to the oxygen chemical potential μ_O by the Gibbs-Duhem relation (at constant temperature and pressure):

$$\mathbf{2d}\mu_{Cr} + \mathbf{3d}\mu_O = \mathbf{0} \qquad \text{Equation 13}$$

And the chemical potential of oxygen is linked to the oxygen pressure by:

$$\mu_O = \mu_O^{\circ} + \frac{\mathbf{1}}{\mathbf{2}}RT\ \mathbf{ln}\, P_{O_2} \qquad \text{Equation 14}$$

Therefore, by combining with Eq. 13 and 14, Eq. 12 becomes on rearrangement:

$$\bar{D}_{Cr} = D^{\bullet}_{Cr}\left(-\frac{3}{4}\frac{N_{Cr}}{P_{O_2}}\frac{dP_{O_2}}{dN_{Cr_i}}\right) \quad \text{Equation 15}$$

Now if we consider the formation of chromium interstitials, their concentration can be expressed as a function of the oxygen pressure. Assuming triply charged defects and electronic defects predominance, this concentration is expressed by Eq. 16 [11].

$$N_{Cr_i} = \left(\frac{K_{Cr_i}}{K_i^{3/2}}\right)P_{O_2}^{-3/4} \quad \text{Equation 16}$$

where K_{Cr_i} is the equilibrium constant for the formation reaction of chromium interstitials and K_i is the equilibrium constant for intrinsic ionization. By inserting Eq. 16 and its derivate form in Eq. 15 in order to replace the terms P_{O_2} and dP_{O_2}, the relation between the intrinsic diffusion coefficient and the tracer diffusion coefficient becomes on rearrangement:

$$N_{Cr_i}\bar{D}_{Cr} = N_{Cr}D^{\bullet}_{Cr} \quad \text{Equation 17}$$

By inserting Eq. 17 in Eq. 8, and since Ω is the inverse of N_{Cr}, it appears that the parabolic rate constant k_{pe} is equal to the tracer diffusion coefficient of chromium in the oxide layer D^{*}_{Cr}. This is a specific case where the oxide is an electronic semi-conductor. For the case of ionic semi-condition, a similar development as above would result in a modification of Eq. 17 to the following form:

$$N_{Cr_i}\bar{D}_{Cr} = (1+z)N_{Cr}D^{\bullet}_{Cr} \quad \text{Equation 18}$$

where z is the effective charge of the diffusing chromium interstitial species.

Therefore from Eq. 17 and Eq. 8, the tracer diffusion coefficient of chromium D^{*}_{Cr} is calculated and found equal to 5.0 x 10^{-12} cm^2 s^{-1}. This value is close to the one obtained by Hagel and Seybolt's work on sintered Cr_2O_3 polycrystals [69] (2.4 x 10^{-12} cm^2 s^{-1}) and is in perfect agreement with the one from Kofstad and Lillerud [68]. Indeed, they calculated the variation with temperature of the self-diffusion coefficient of chromium, with the same model applied as in the present study (diffusion by interstitials in electronic defect predominance) [68]. Their calculations led to:

$$D_{Cr} = 5.0 \times 10^{-3}\exp\left(-\frac{245{,}000}{RT}\right) \quad \text{Equation 19}$$

At 1150 °C, Eq. 19 gives a self-diffusion coefficient equal to 5.1 x 10^{-12} cm^2 s^{-1}, close to the value determined in this work.

In conclusion, based on the data on the oxidation kinetics, the tracer diffusion coefficient of chromium in Cr_2O_3 oxide layer has been determined at 1150 °C and is equal to 5.0 x 10^{-12} cm^2 s^{-1}. Such high value is representative of diffusion along short-path circuits (Fig. 13), which is consistent with the fine microstructure of the oxide (Fig. 3).

3.3. Defects concentration

Finally, the objective of this last section is to determine the defects concentration at the alloy/oxide interface, N_{Cr_i}, from data in literature and from the calculated chromium permeability in Cr_2O_3 (Table 3).

A few data are available in literature on the defects concentration in Cr_2O_3: Su and Simkovich have determined via conductivity measurement a defects concentration around 10^{18} at cm^{-3} at 1100 °C [43]. Vaari has estimated, from molecular dynamics simulations, defects concentrations varying from 10^3 up to 10^{15} at cm^{-3} depending on the formation energy that had been used for computing [72]. However, if their values are used with the previously determined permeability ($N_{Cr_i}.\bar{D}_{Cr}$ = 2 x 10^{11} at cm^{-1}) to calculate $\bar{D}_{Cr}$, results would be several orders of magnitude higher than any reported diffusion coefficient (Fig. 13).

Liu *et al.* have measured the concentration of chromium interstitials in a Cr_2O_3 scale grown on Ni-20Cr substrate by asymmetry polarization technique [73]. The extrapolation at 1150 °C of their results gives a chromium interstitials concentration of about 10^{21} at cm^{-3}, which represents 2.5% of the total amount of chromium in Cr_2O_3. Calculation made with this value and the chromium permeability in Cr_2O_3 (Table 3) gives an intrinsic chromium diffusion coefficient $\bar{D}_{Cr}$ of about 2 x 10^{-10} cm^2 s^{-1}. This value is comprised between (i) the extrapolated intrinsic diffusion coefficient along grain boundaries from Tsaï *et al.* [16] (5.2 x 10^{-10} cm^2 s^{-1}), which reflects a vacancy mechanism, and (ii) the one obtained by Hagel and Seybolt on hot-pressed Cr_2O_3 samples [68] (5.55 x 10^{-11} cm^2 s^{-1}), which reflects an interstitial mechanism. Therefore, the extrapolation of the results of Liu *et al.* [73] makes a reasonable approximation of the chromium interstitials concentration in the oxide near the alloy/oxide phase boundary.

Conclusions

A specific technique previously unseen for the study of external oxidation of alloys has been implemented. Oxidation tests of binary Ni-30Cr alloy have been carried out in several intermediate oxygen partial pressures in Rhines packs at 1150 °C. Thanks to this method the sole oxide growth kinetics of Cr_2O_3 is achieved, without volatilisation phenomenon and without disruption by hydrogen or carbon presence in the oxidising atmosphere. Oxide morphology, growth kinetics and mechanisms have been assessed in terms of nature, concentration and diffusion of point defects. The effect of the oxygen pressure on the oxidation kinetics and mechanism has been discussed based on this work and on reviews of the literature for parabolic rate constant of oxidation of Ni-Cr alloys and for the concentration and diffusion coefficient of point defects in Cr_2O_3.

The presented results have shown that:

1. The mechanical properties of the oxide layer are dependent on the oxygen pressure. Higher oxygen pressures induce increased growth stresses in the oxide due to enhanced diffusion of oxygen.
2. The oxidation kinetics of Ni-30Cr alloy at 1150 °C is independent on the oxygen pressure in a $P(O_2)$ range from 10^{-13} up to 10^{-3} atm. The mean value of the parabolic rate constant k_{pe} has been found to be equal to 5.0×10^{-12} cm^2 s^{-1}.
3. Based on inert markers experiments, it has been shown that the Cr_2O_3 oxide grows mainly by outward diffusion of chromium at 1150 °C in a $P(O_2)$ range from 10^{-13} up to 10^{-3} atm.
4. From these results, it has been deduced that the oxide growth kinetics is controlled by diffusion of chromium interstitials at 1150 °C in a $P(O_2)$ range from 10^{-13} up to 10^{-3} atm.
5. The transition between chromium interstitial and chromium vacancy type mechanism for oxidation is drawn depending on temperature and external oxygen pressure.
6. The chromium permeability in Cr_2O_3 scale at 1150 °C is equal to about 2×10^{11} at cm^{-1} s^{-1}.
7. The chromium tracer diffusion coefficient in Cr_2O_3 layer at 1150 °C is calculated from oxidation kinetics data and is equal to 5×10^{-12} cm^2 s^{-1}.
8. The chromium interstitials concentration in Cr_2O_3 layer grown on Ni-Cr alloy at 1150 °C, N_{Cr_i}, is approximated to 10^{21} at cm^{-3} [73].

Acknowledgements

The authors are grateful to P. Boulet for performing high temperature XRD measurement and to S. Mathieu for her helpful contribution in SEM characterisations.

References

[1] P. Sengupta, Interaction study between nuclear waste-glass melt and ceramic melter bellow liner materials. J. Nucl. Mater. 411 (2011) 181-184.

[2] J.R. Davis (Ed.), Nickel, cobalt, and their alloys. ASM international, 2000.

[3] P. Berthod, L. Aranda, Thermal expansion behaviour of ternary nickel-based, cobalt-based, and iron-based alloys containing very high fractions of carbides, ISRN Metall. 2012, (2012) 1-9.

[4] H.V. Atkinson, A review of the role of short-circuit diffusion in the oxidation of nickel, chromium, and nickel-chromium alloys, Oxid. Met. 24 (1985) 177-197.

[5] H. Davies, W.W. Smeltzer, Oxygen and metal activities of the chromium-nickel-oxygen system between 900° and 1100°C, J. Electrochem. Soc. 121 (1974) 543-549.

[6] E. Essuman, G.H. Meier, J. Zurek, M. Hänsel, T. Norby, L. Singheiser, W.J. Quadakkers, Protective and non-protective scale formation of NiCr alloys in water vapour containing high- and low-pO_2 gases, Corros. Sci. 50 (2008) 1753-1760.

[7] C. Wagner, Beitrag zur theorie des anlaufvorgangs, Z. Phys. Chem. B 21 (1933) 25-41.

[8] P. Berthod, Kinetics of high temperature oxidation and chromia volatilization for a binary Ni–Cr alloy, Oxid. Met. 64 (2005) 235-252.

[9] E.J. Opila, Volatility of common protective oxides in high-temperature water vapor: current understanding and unanswered questions, Mater. Sci. For. 461 (2004) 765-774.

[10] R. Sachitanand, J.E. Svensson, J. Froitzheim, The influence of Cr evaporation on long term Cr depletion rates in ferritic stainless steels, Oxid. Met. 84 (2015) 241-257.

[11] P. Kofstad, High Temperature Corrosion. Elsevier, London, 1988.

[12] H. Hindam, D.P. Whittle, Microstructure, adhesion and growth kinetics of protective scales on metals and alloys, Oxid. Met. 18 (1982) 245-284.

[13] H. Beske, W.J. Quadakkers, H. Holzbrecher, H. Schuster, H. Nickel, SIMS investigations on the growth mechanisms of protective chromia and alumina surface scales, Mikrochim. Acta 101 (1990) 109-119.

[14] G.M. Ecer, G.H. Meier, Oxidation of high-chromium Ni-Cr alloys, Oxid. Met. 13 (1979) 119-158.

[15] J. Zurek, D.J. Young, E. Essuman, M. Hänsel, H.J. Penkalla, L. Niewolak, W.J. Quadakkers, Growth and adherence of chromia based surface scales on Ni-base alloys in high-and low-pO_2 gases, Mater. Sci. Eng., A 477 (2008) 259-270.

[16] S.C. Tsai, A.M. Huntz, C. Dolin, Growth mechanism of Cr_2O_3 scales: oxygen and chromium diffusion, oxidation kinetics and effect of yttrium. Mater. Sci. Eng., A 212 (1996) 6-13.

[17] S. Henry, J. Mougin, Y. Wouters, J.P. Petit, A. Galerie, Characterization of chromia scales grown on pure chromium in different oxidizing atmospheres. Mater. High Temp. 17 (2000) 231-234.

[18] P. Kofstad, K.P. Lillerud, On high temperature oxidation of chromium II. Properties of Cr_2O_3 and the oxidation mechanism of chromium. J. Electrochem. Soc. 127 (1980) 2410-2419.

[19] S.C. Tsai, A.M. Huntz, C. Dolin, C. Monty, Study by SIMS of the ^{54}Cr and ^{18}O diffusion in Cr_2O_3 and in Cr_2O_3 scales, Mikrochim. Acta S13 (1996) 587-595.

[20] A.C.S. Sabioni, A.M. Huntz, J. Philibert, B. Lesage, C. Monty, Relation between the oxidation growth rate of chromia scales and self-diffusion in Cr_2O_3, J. Mater. Sci. 27 (1992) 4782-4790.

[21] T. Norby, Protonic defects in oxides and their possible role in high temperature oxidation. J. Phys. IV 3 (1993) 99-106.

[22] T.A. Ramanarayanan, M. Raghavan, R. Petkovic-Luton, Metallic yttrium additions to high temperature alloys: Influence on Al_2O_3 scale properties, Oxid. Met. 22 (1984) 83-100.

[23] H. Hindam, D.P. Whittle, Evidence for the growth mechanism of Cr_2O_3 at low oxygen potentials, J. Electrochem. Soc. 130 (1983) 1519-1523.

[24] T.A. Ramanarayanan, J.D. Mumford, C.M. Chun, R.A. Petkovic, Transport through chromia films, Solid State Ionics 136 (2000) 83-90.

[25] S. Guillou, C. Cabet, C. Desgranges, L. Marchetti, Y. Wouters, Influence of hydrogen and water vapour on the kinetics of chromium oxide growth at high temperature, Oxid. Met. 76 (2011) 193-214.

[26] T. Gheno, G.H. Meier, B. Gleeson, High Temperature Reaction of MCrAlY Coating Compositions with CaO Deposits, *Oxid. Met.* 84 (2015) 185-209.

[27] F.N. Rhines, A metallographic study if internal oxidation in the alpha solid solutions of copper, *Trans. Met. Soc. AIME*, 137 (1940) 246-286.

[28] G.C. Wood, F.H. Stott, D.P. Whittle, Y. Shida, B.D. Bastow, The high-temperature internal oxidation and intergranular oxidation of nickel-chromium alloys, Corros. Sci. 23 (1983) 9-25.

[29] F.H. Stott, G.C. Wood, D.P. Whittle, B.D. Bastow, Y. Shida, A. Martinez-Villafane, The transport of oxygen to the advancing internal oxide front during internal oxidation of nickel-base alloys at high temperature, *Solid State Ionics*, 12 (1984) 365-374.

[30] P. Guo, J. Zhang, D.J. Young, C.H. Konrad, Oxygen Permeability Measurements in Ni Using H_2/H_2O, CO/CO_2 and Ni/NiO Rhines Pack Atmospheres, *Oxid. Met.* 83 (2015) 223-235.

[31] W. Huang, Y.A. Chang, Thermodynamic properties of the Ni–Al–Cr system, Intermetallics 7 (1999) 863-874.

[32] E. Schmucker, C. Petitjean, L. Martinelli, P.J. Panteix, S. Ben Lagha, M. Vilasi, Oxidation of Ni-Cr alloy at intermediate oxygen pressures. II. Chromium depletion in the alloy, Submitted to Corros. Sci. (2016)

[33] A. Roine, HSC chemistry for Windows, version 5.1, 1999. Outokompu Research Oy, Pori, Finland.

[34] I. Barin, Thermochemical Data of Pure Substances, VCH, Weinheim, 1993.

[35] I. Barin, Thermochemical Data of Pure Substances, VCH, Weinheim, 1989.

[36] O.B. Fabrichnaya, The phase relations in the FeO-MgO-Al_2O_3-SiO_2 system: assessment of thermodynamic properties and phase equilibria at pressures up to 30 GPa, Calphad, 23 (1999) 19-67.

[37] H. Landolt, R. Börnstein, Thermodynamic Properties of Inorganic Material, Springer, Berlin, 1999.

[38] J. Malcolm, NIST-JANAF Thermochemical Tables, fourth ed., AIP 1998.

[39] C.S. Giggins, F.S. Pettit, Oxidation of Ni-Cr alloys between 800 and 1200°C, Trans. Met. Soc. AIME 245 (1969) 2495-2507.

[40] H.F. McMurdie, M.C. Morris, E.H. Evans, B. Paretzkin, W. Wong-Ng, Y. Zhang, C.R. Hubbard, Standard X-ray diffraction powder patterns from the JCPDS research associateship. Powder diffraction 2 (1987) 41-52.

[41] D. Monceau, B. Pieraggi, Determination of parabolic rate constants from a local analysis of mass-gain curves, Oxid. Met. 50 (1998) 477-493.

[42] A. Holt, P. Kofstad, Electrical conductivity and defect structure of Cr_2O_3. I. High temperatures (> ~ 1000°C), Solid State Ionics 69 (1994) 127-136.

[43] M.Y. Su, G. Simkovich, Point defect structure of chromium (III) oxide, in: J. Nowotny, W. Weppner (Eds.), Non-Stoichiometric Compounds, Springer, 1989, pp. 93-113.

[44] Y. Zhang, D.A. Shores, Study of cracking and spalling of Cr_2O_3 scale formed on Ni-30Cr alloy, Oxid. Met. 40 (1993) 529-553.

[45] M. Kemdehoundja, J.F. Dinhut, J.L. Grosseau-Poussard, M. Jeannin, High temperature oxidation of $Ni_{70}Cr_{30}$ alloy: determination of oxidation kinetics and stress evolution in chromia layers by Raman spectroscopy, Mater. Sci. Eng., A 435 (2006) 666-671.

[46] P. Berthod, L. Aranda, S. Mathieu, M. Vilasi, Influence of water vapour on the rate of oxidation of a Ni–25wt.% Cr alloy at high temperature, Oxid. Met. 79 (2013) 517-527.

[47] H.E. Evans, Cracking and spalling of protective oxide layers, Mater. Sci. Eng., A 120 (1989) 139-146.

[48] T. Maruyama, N. Fukagai, M. Ueda, K. Kawamura, Chemical potential distribution and void formation in magnetite scale formed in oxidation of iron at 823K, Mater. Sci. For. 461 (2004) 807-814.

[49] T. Maruyama, K. Akiba, M. Ueda, K. Kawamura, Void formation in growing oxide scales with Schottky defects and p-type conduction, Mater. Sci. For. 595 (2008) 1039-1046.

[50] B. Li, B. Gleeson, Effects of silicon on the oxidation behavior of Ni-base chromia-forming alloys, Oxid. Met. 65 (2006) 101-122.

[51] X. Ledoux, S. Mathieu, M. Vilasi, Y. Wouters, P. Del-Gallo, M. Wagner, Oxide growth characterization during short-time oxidation of a commercially available chromia-forming alloy (HR-120) in air at 1,050° C, Oxid. Met. 80 (2013) 25-35.

[52] A. Chyrkin, W.G. Sloof, R. Pillai, T. Galiullin, D. Grüner, L. Singheiser, W.J. Quadakkers, Modelling compositional changes in nickel base alloy 602 CA during high temperature oxidation, Mater. High Temp. 32 (2015) 102-112.

[53] P. Moulin, A.M. Huntz, P. Lacombe, Influence des phénomènes diffusionnels sur le mécanisme d'oxydation des alliages Ni-Cr, Acta Metall. 28 (1980) 745-756.

[54] G. Calvarin, R. Molins, A.M. Huntz, Oxidation mechanism of Ni—20Cr foils and its relation to the oxide-scale microstructure, Oxid. Met. 53 (2000) 25-48.

[55] T. Hodgkiess, G.C. Wood, D.P. Whittle, B.D. Bastow, The oxidation of Ni-70 wt.% Cr in oxygen between 1073 and 1473° K, Oxid. Met. 14 (1980) 263-277.

[56] G.C. Wood, I.G. Wright, T. Hodgkiess, D.P. Whittle, A comparison of the oxidation of Fe-Cr, Ni-Cr and Co-Cr alloys in oxygen and water vapour, Mater. Corros. 21 (1970) 900-910.

[57] M. Hänsel, V. Shemet, E. Turan, I. Kijatkin, D. Simon, B. Gorr, H.J. Christ, Scaling kinetics and scale microstructure of chromia scales formed on Ni-%25Cr model alloy during oxidation in H_2O-containing high and low pO_2 test gas at 1000°C, ECS Trans. 66 (2015) 1-21.

[58] H.T. Michels, The effect of dispersed reactive metal oxides on the oxidation resistance of nickel-20 wt pct chromium alloys, Metall. Trans., A 7 (1976) 379-388.

[59] B. Sundman, B. Jansson, J.O. Andersson, The thermo-calc databank system, Calphad 9 (1985) 153-190.

[60] M. Moeglen, Modification de la réactivité de surface d'un alliage base nickel afin de limiter le relâchement du nickel en milieu primaire des réacteurs à eau pressurisée, PhD Thesis, Université de Grenoble, France, 2015.

[61] D.J. Young, High Temperature Oxidation and Corrosion of Metals, Elsevier, Amsterdam, 2008.

[62] A.C.S. Sabioni, B. Lesage, A.M. Huntz, J.C. Pivin, C. Monty, Self-diffusion in Cr_2O_3 I. Chromium diffusion in single crystals. Philos. Mag. A 66 (1992) 333-350.

[63] A. Atkinson, R.I. Taylor, Diffusion of ^{51}Cr Tracer in Cr_2O_3 and the Growth of Cr_2O_3 Films, in: G. Simkovich, V.S. Stubican (Eds.), Transport in Non-Stoichiometric Compounds, Springer, 1985, pp. 93-113.

[64] K. Hoshino, N.L. Peterson, Cation self-diffusion in Cr_2O_3, J. Am. Ceram. Soc. 66 (1983) c202-c203.

[65] F. Lebreau, M.M. Islam, B. Diawara, P. Marcus, Structural, magnetic, electronic, defect, and diffusion properties of Cr_2O_3: A DFT+ U study, J. Phys. Chem. C 118 (2014) 18133-18145.

[66] A.C.S. Sabioni, A.M. Huntz, F. Millot, C. Monty, Self-diffusion in Cr_2O_3 III. Chromium and oxygen grain-boundary diffusion in polycrystals, Philos. Mag. A 66 (1992) 361-374.

[67] J.H. Park, W.E. King, S.J. Rothman, Cation tracer diffusion in Cr_2O_3 and Cr_2O_3-0.09 wt% Y_2O_3, J. Am. Ceram. Soc. 70 (1987) 880-885.

[68] P. Kofstad, K.P. Lillerud, Chromium transport through Cr_2O_3 scales I. On lattice diffusion of chromium, Oxid. Met. 17 (1982) 177-194.

[69] W.C. Hagel, A.U. Seybolt, Cation diffusion in Cr_2O_3, J. Electrochem. Soc. 108 (1961) 1146-1152.

[70] M. Kizilyalli, J. Corish, R. Metselaar, Definitions of terms for diffusion in the solid state, Pure Appl. Chem. 71 (1999) 1307-1325.

[71] H. Mehrer, Diffusion in Solids: Fundamentals, Methods, Materials, Diffusion-controlled Processes, Springer, Berlin, 2007.

[72] J. Vaari, Molecular dynamics simulations of vacancy diffusion in chromium (III) oxide, hematite, magnetite and chromite, Solid State Ionics 270 (2015) 10-17.

[73] H. Liu, M.M. Stack, S.B. Lyon, Reactive element effects on the ionic transport processes in Cr_2O_3 scales, Solid State Ionics 109 (1998) 247-257.

Table 1: Metal/oxide and oxide/oxide buffers used in the Rhines pack and their corresponding equilibrium pressure of oxygen and chromium oxide at 1150 °C

Buffer	***P*(O_2) (atm)**	***P*(CrO_3) (atm)**	**Database**
Fe_2O_3 / Fe_3O_4	5.9×10^{-3}	5.0×10^{-8}	[34,35]
Fe_3O_4 + SiO_2 / Fe_2SiO_4	4.2×10^{-10}	2.2×10^{-13}	[34-36]
Fe_3O_4 / FeO	5.8×10^{-12}	8.8×10^{-15}	[34,35,37]
FeO / Fe	2.8×10^{-13}	9.1×10^{-16}	[34,37]

Table 2: Parabolic rate constants for the oxidation of Ni-30Cr alloy at 1150 °C in different oxygen partial pressures

$P(O_2)$ (atm)	2.8×10^{-13}	5.8×10^{-12}	4.2×10^{-10}	5.9×10^{-3}
k_{pe} ($cm^2\ s^{-1}$)	4.3×10^{-12}	6.9×10^{-12}	5.1×10^{-12}	3.8×10^{-12}

Table 3: Key parameters summarising the oxide growth kinetics on Ni-30Cr at 1150 °C in 10^{-13} up to 10^{-3} atm O_2

Parameters	Symbols	Values	Units	References
Parabolic rate constant	k_{pe}	5×10^{-12}	$cm^2\ s^{-1}$	This work
Cr permeability in Cr_2O_3	$N_{Cr_i}.\bar{D}_{Cr}$	2×10^{11}	at cm^{-1}	This work
Cr tracer diffusion coefficient or self-diffusion coefficient in Cr_2O_3	D^*_{Cr} or D_{Cr}	5×10^{-12}	$cm^2\ s^{-1}$	This work, [68]
Cr interstitials in Cr_2O_3 at the alloy/oxide interface	N_{Cr_i}	1×10^{21}	at cm^{-3}	[73]
Cr intrinsic diffusion coefficient in Cr_2O_3	$\bar{D}_{Cr}$	2×10^{-10}	$cm^2\ s^{-1}$	This work

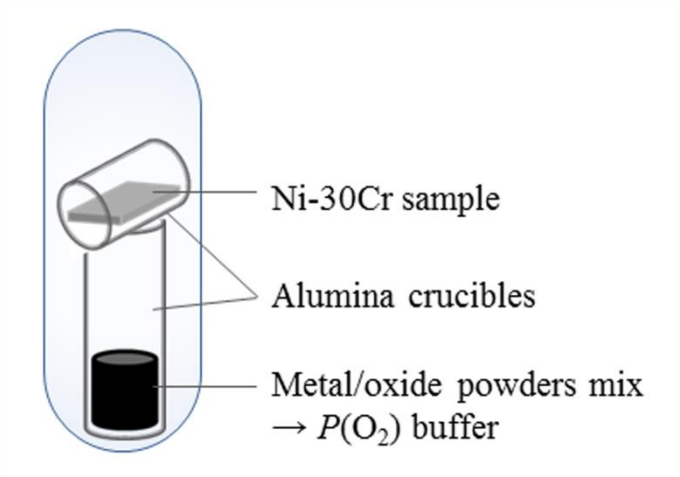

Figure 1: Rhines pack device for oxidation tests

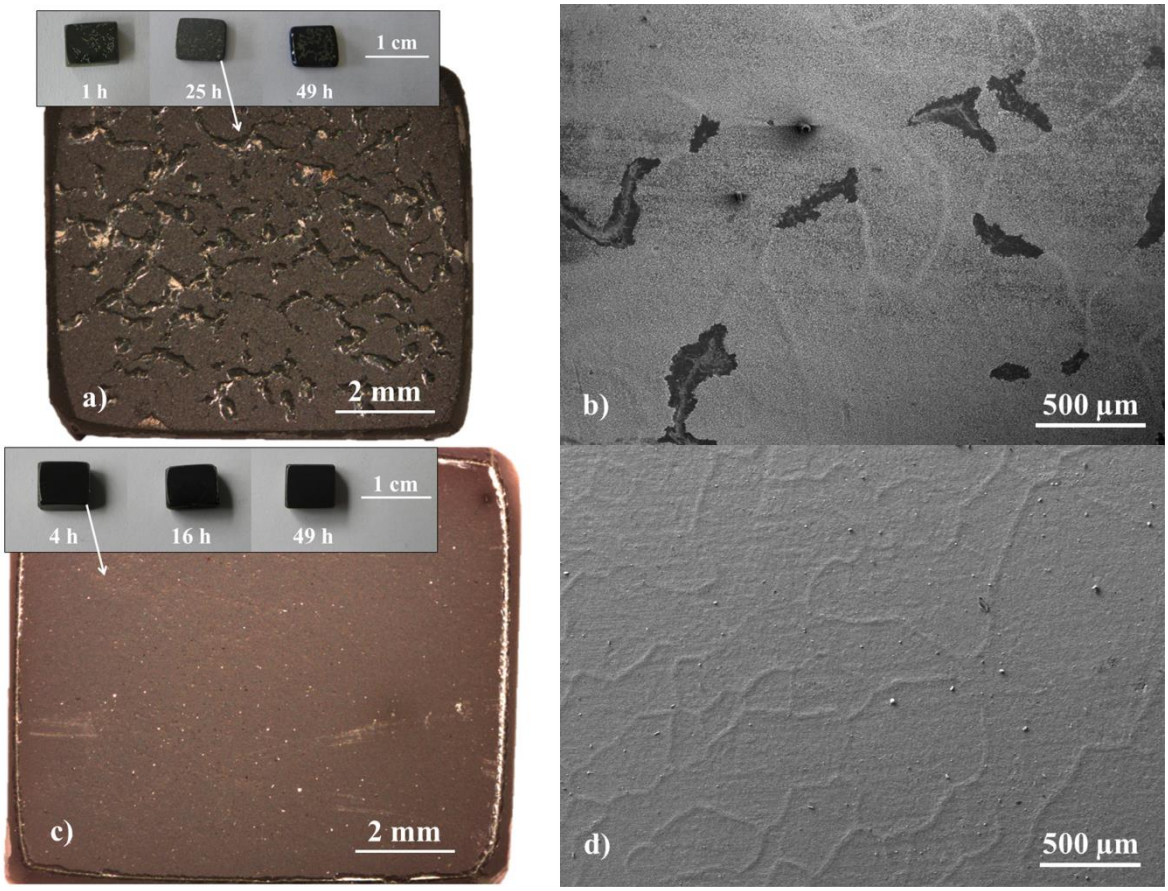

Figure 2: (a) Optical image of a Ni-30Cr samples oxidised in 5.9 x 10^{-3} atm O_2; (b) SE image of the surface of Ni-30Cr oxidised for 9 h in 5.9 x 10^{-3} atm O_2; (c) Optical image of Ni-30Cr samples oxidised in 4.2 x 10^{-10} atm O_2; (d) SE image of the surface of Ni-30Cr oxidised for 4 h in 5.8 x 10^{-12} atm O_2

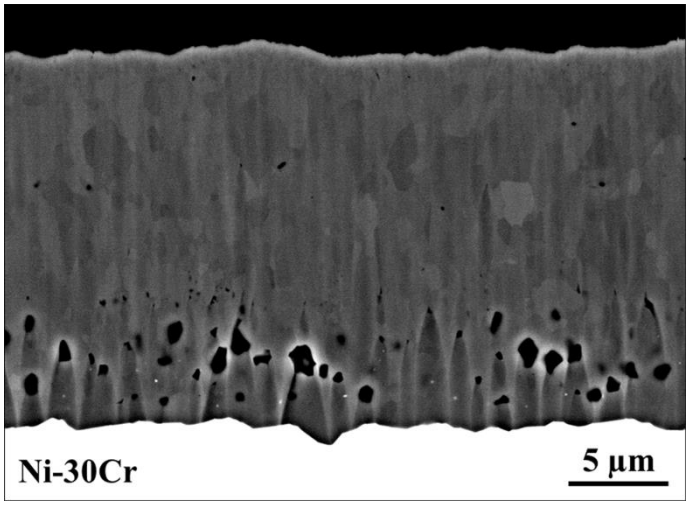

Figure 3: Cross-section BSE image of the oxide scale formed on Ni-30Cr oxidised for 49 h in 5.9 x 10^{-3} atm O_2

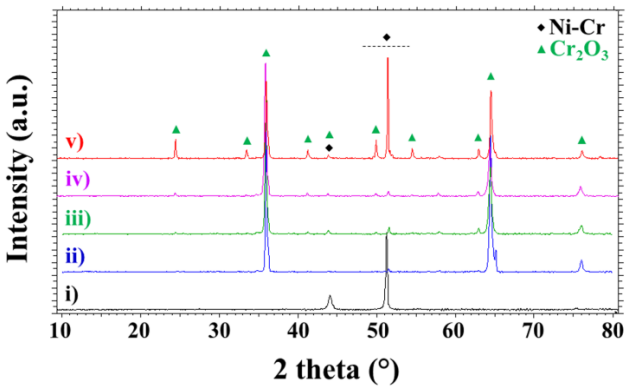

Figure 4: Diffractogram ($\lambda_{CuK\alpha1}$ = 1.5406 Å) of i) as-prepared Ni-30Cr alloy, ii) oxidised for 16 h in 2.8 x 10^{-13} atm O_2, iii) oxidised for 4 h in 5.8 x 10^{-12} atm O_2, iv) oxidised for 25 h in 4.2 x 10^{-10} atm O_2, v) oxidised for 49 h in 5.9 x 10^{-3} atm O_2

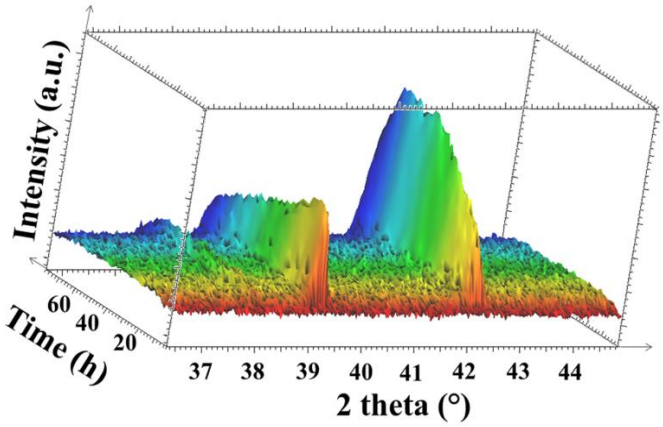

Figure 5: Diffractogram ($\lambda_{CoK\alpha1}$ = 1.7900 Å) showing the evolution of (104) peak (left) and (110) peak (right) of Cr_2O_3 on Ni-30Cr with increasing time at 1100 °C in air

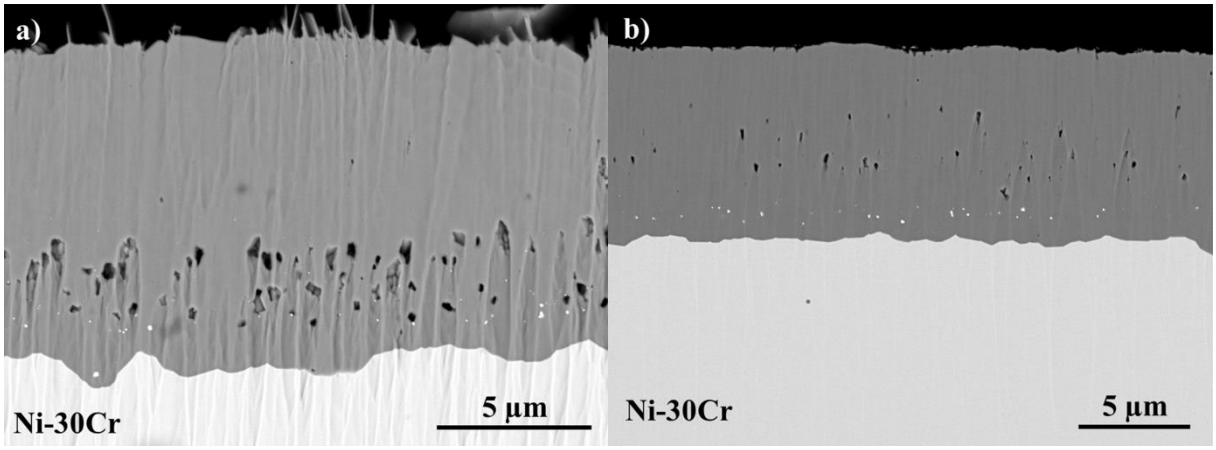

Figure 6: BSE image of the oxide scale formed with inert markers on Ni-30Cr oxidised for 9 h in (a) 5.9 x 10^{-3} atm O_2; (b) 2.8 x 10^{-13} atm O_2

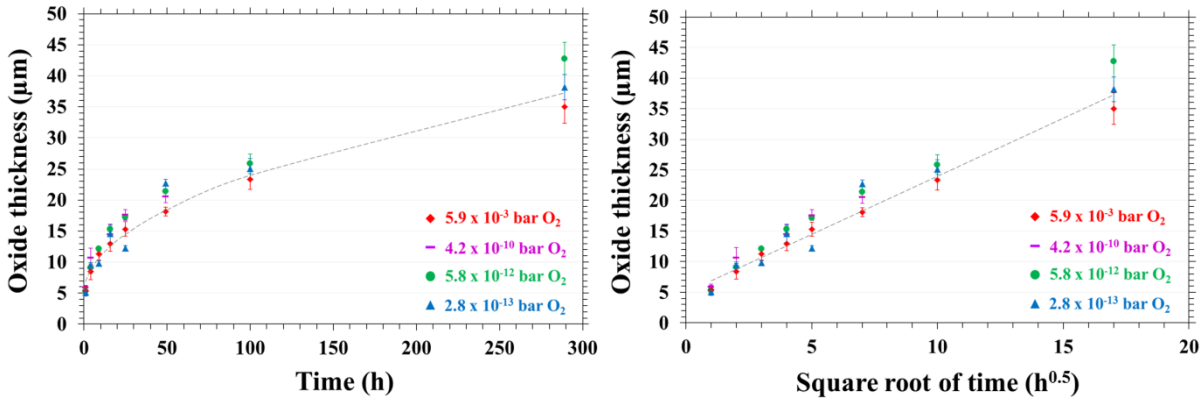

Figure 7: Evolution of the Cr_2O_3 thickness on Ni-30Cr oxidised at 1150 °C in the different tested partial pressures of oxygen: (a) thickness *vs.* time (dashed lines represents parabolic curve with k_{pe} = 5.0 x 10^{-12} cm^2 s^{-1}) and (b) thickness *vs.* square root of time showing the parabolic behaviour (dashed line is traced with a slope equal to $\sqrt{(2*k_{pe})}$)

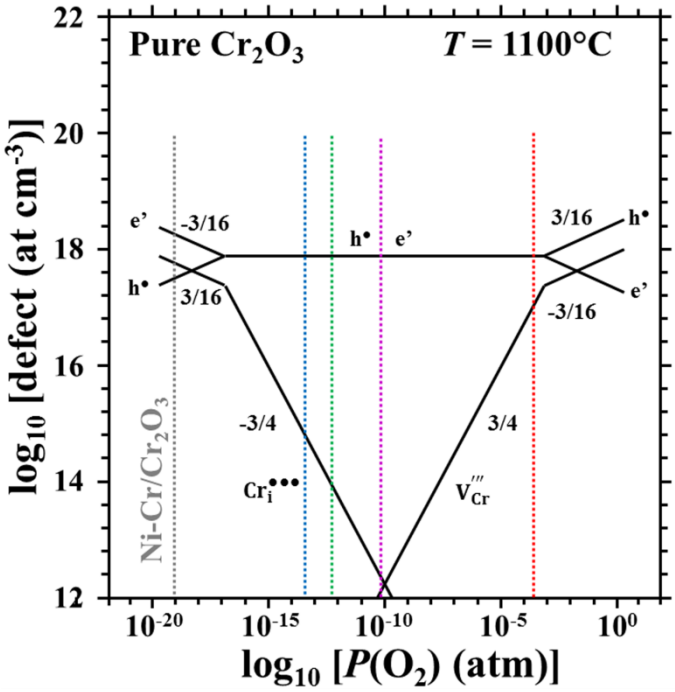

Figure 8: Brouwer diagram of Cr_2O_3 according to [43]. Dotted lines indicates the partial pressures of oxygen that would be imposed at 1100 °C by $P(O_2)$ buffers used in this work

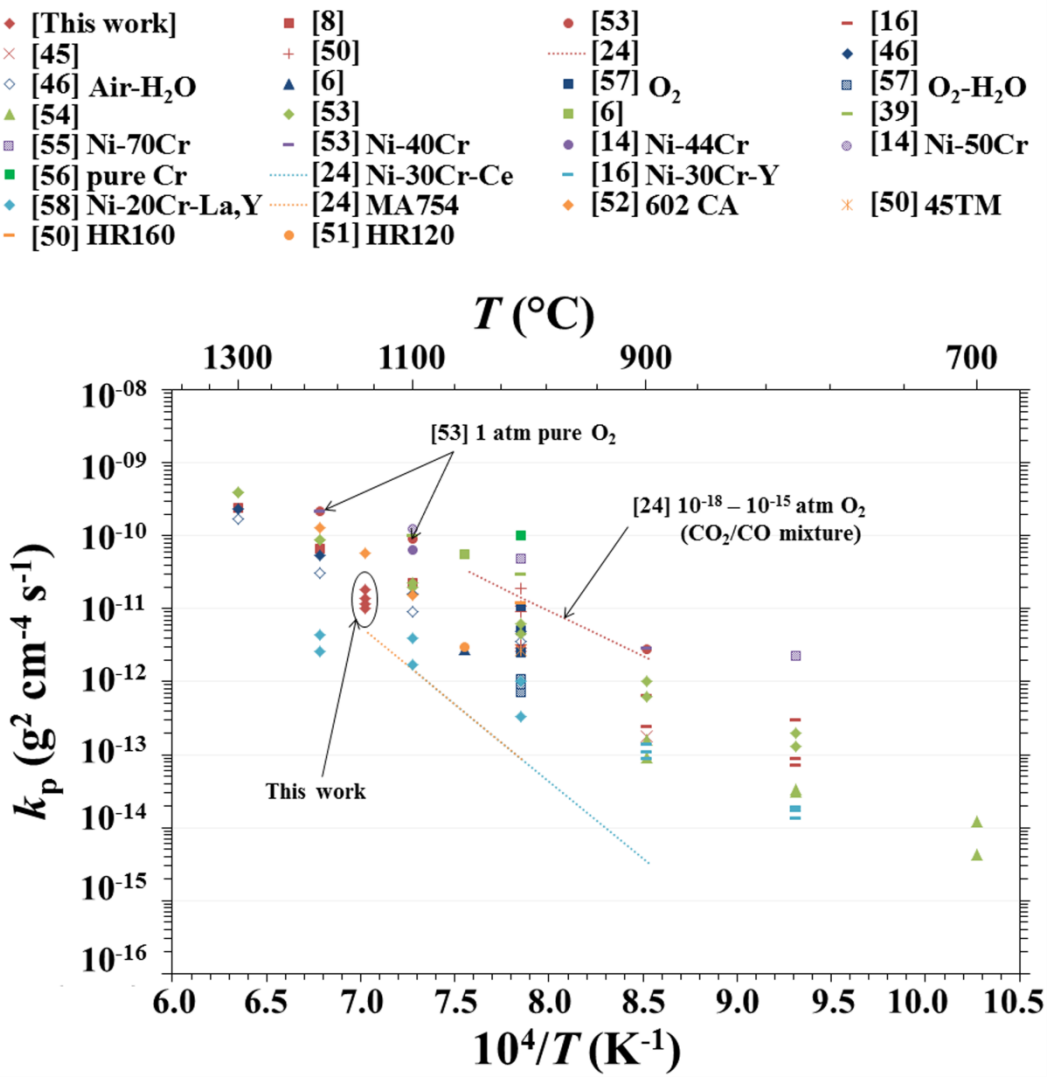

Figure 9: (colours online) Arrhenius representation of k_p values for the oxidation of Ni-based chromia-forming alloys from literature and this work. (**Red** symbols are for Ni-30Cr; **dark blue** for Ni-25Cr; **light green** for Ni-20Cr; **purple** for high chromium alloys; **light blue** for Ni-Cr with reactive elements addition and **orange** for commercial alloys)

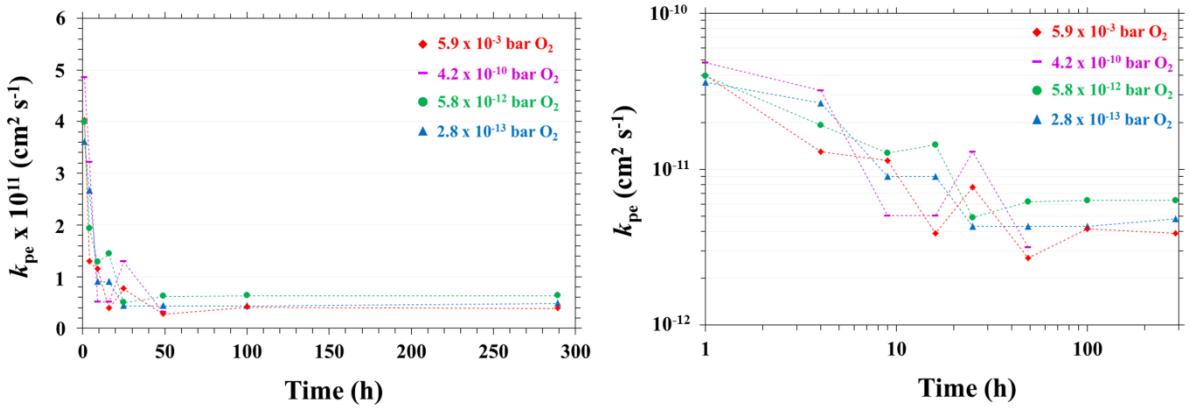

Figure 10: Evolution of the parabolic rate constants for the oxidation of Ni-30Cr at 1150 °C in different oxygen partial pressures: (a) k_{pe} vs. time and (b) logarithmic representation of k_{pe} vs. time

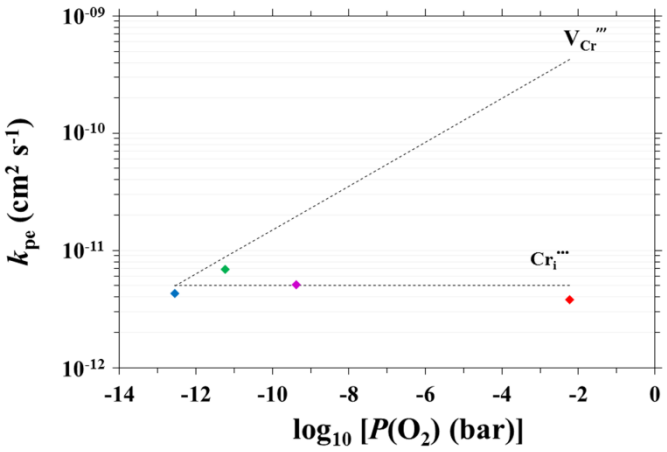

Figure 11: Plot of experimentally determined parabolic rate constants versus oxygen partial pressure for the oxidation of Ni-30Cr alloy at 1150 °C (dashed line represents the evolution tendencies of k_{pe} values depending on which type of defect is considered)

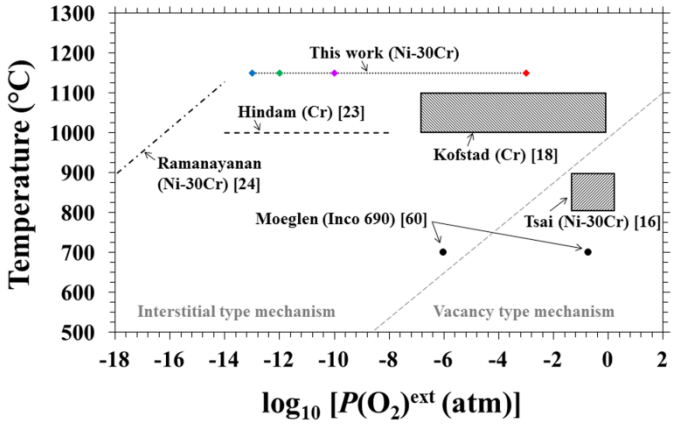

Figure 12: Diffusion mechanisms (interstitial or vacancy type) determined in this work and by others authors for the oxidation of chromia-formers as a function of temperature and external oxygen pressure.

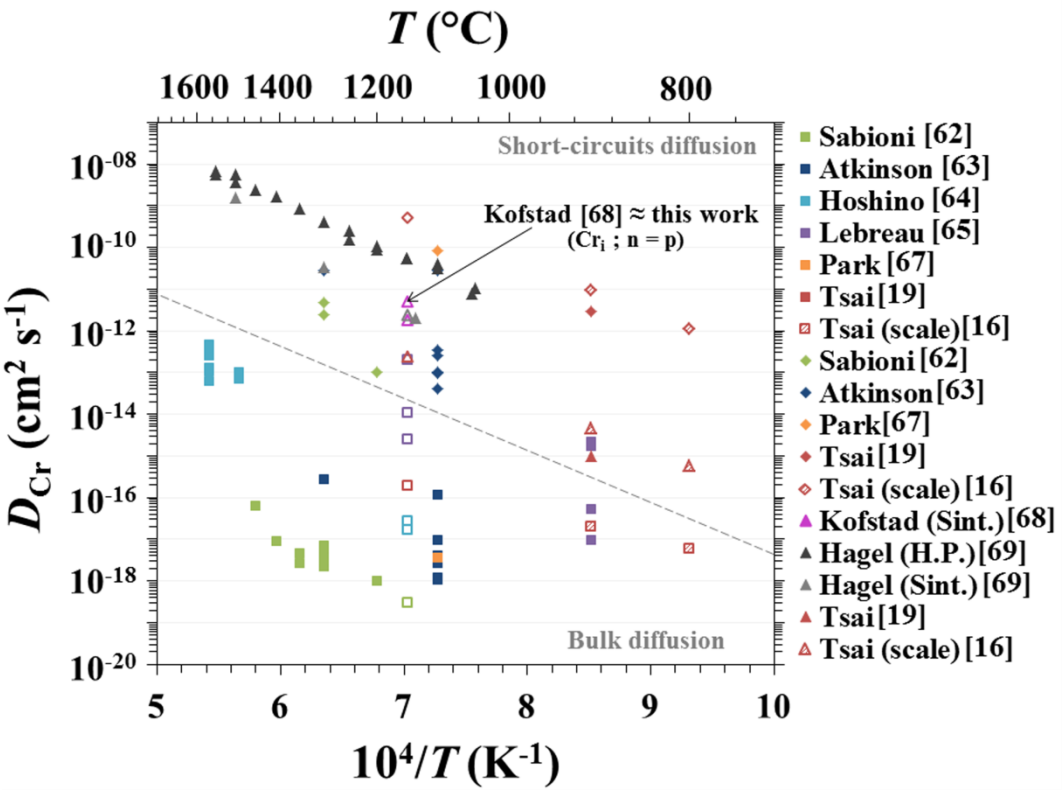

Figure 13: (colours online) Arrhenius representation of the diffusion coefficients of chromium in Cr_2O_3 from literature. (Square symbols represent bulk diffusion coefficients, diamond shaped symbols represent short-circuits diffusion coefficients and triangles represent mixed diffusion coefficients. Empty symbols are values at 1150 °C calculated from activation energies and pre-exponential factors)